AD-A165 691 THE ESTIMATION OF GEOPOTENTIALS BY WAY OF GEOPHYSICAL INVERSE THEORY(U) MASSACHUSETTS INST OF TECH LEXINGTON LINCOLN LAB M T LANE ET AL. 27 JAN 86 TR-735 1/1

UNCLASSIFIED ESD-TR-85-279 F19628-85-C-0002 F/G 8/5 NL

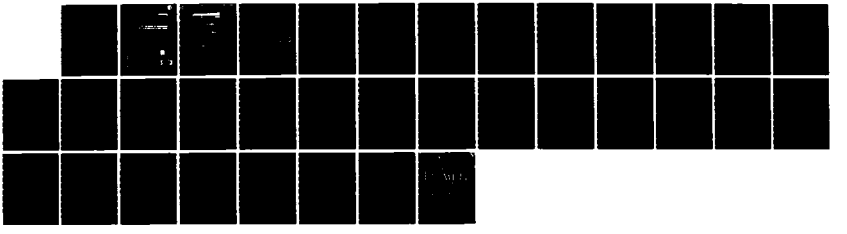

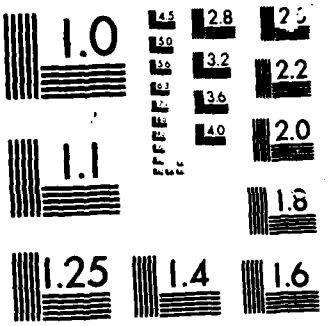

ESD-TR-85-279

Technical Report
735

The Estimation of Geopotentials by Way of Geophysical Inverse Theory

M.T. Lane
E.M. Gaposchkin

27 January 1986

Lincoln Laboratory
MASSACHUSETTS INSTITUTE OF TECHNOLOGY
LEXINGTON, MASSACHUSETTS

Prepared for the Department of the Air Force
under Electronic Systems Division Contract F19628-85-C-0002.

The work reported in this document was performed at Lincoln Laboratory, a center for research operated by Massachusetts Institute of Technology, with the support of the Department of the Air Force under Contract F19628-85-C-0002.

This technical report has been reviewed and is approved for publication.

FOR THE COMMANDER

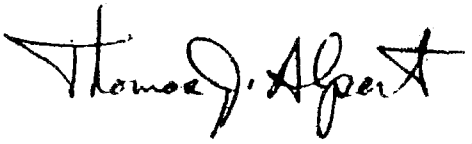

Thomas J. Alpert, Major, USAF
Chief, ESD Lincoln Laboratory Project Office

MASSACHUSETTS INSTITUTE OF TECHNOLOGY
LINCOLN LABORATORY

THE ESTIMATION OF GEOPOTENTIALS BY WAY OF GEOPHYSICAL INVERSE THEORY

M.T. LANE
E.M. GAPOSCHKIN

Group 91

TECHNICAL REPORT 735

27 JANUARY 1986

LEXINGTON MASSACHUSETTS

ABSTRACT

Satellite to Satellite Tracking data (SST) can be used to measure the geopotential at the satellite altitude. This measurement can be used to estimate the Earth's gravity field at the Earth's surface, the so-called "inverse problem." Geophysical inverse theory is applied to this inverse problem, and numerical methods are developed and tested. Geophysical inverse theory is used to map the geopotential from the satellite altitude to a lower surface. Two configurations are explored and the geopotential in a local network is recovered with less than 4% error.

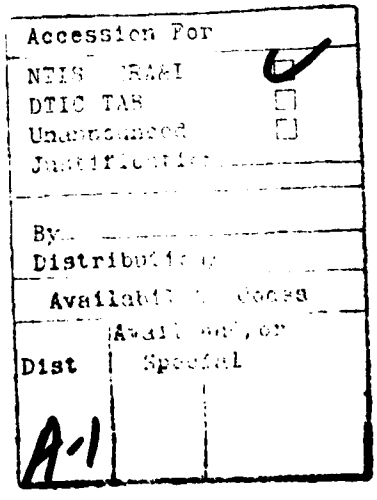

TABLE OF CONTENTS

LIST OF ILLUSTRATIONS

THE ESTIMATION OF GEOPOTENTIALS BY WAY OF GEOPHYSICAL INVERSE THEORY

I. INTRODUCTION

In general, inverse theory begins with an integral equation

$$f(x) = \int g(x,y)\, u(y)\, dy \tag{1}$$

where the kernel g(x,y) is given a priori, and x and y may be vectors. When u(y) is known, f(x) is determined by simple integration methods and is known as the "forward problem." Conversely, when f(x) is given, one seeks to determine u(y) which is known as the "inverse problem." In our case, f(x) is not known everywhere, and therefore we can only hope to obtain a less complete description of u(y). Nevertheless, one can develop a mathematical structure that allows the maximum information (in some sense) to be obtained from a given set of data and a quantification of the quality of the result. Such a formalism has been developed by seismologists in solid earth geophysics, and is known as "geophysical inverse theory."

Geophysical inverse theory has made a profound impact on the study of the Earth's interior. The reader is encouraged to see Reference 1 or 2 for an overview of the theory and how it has been useful in the geophysical context. A motivation for geophysical inverse theory is that much of our knowledge of the Earth's interior is based on observations made at the surface. This is opposite to the forward problem in which a valid mathematical model is constructed from which the behavior of the interior can be calculated directly. Inverse theory is usually not capable of extracting information that is not intrinsically contained in the data, and therefore, the theory is extremely sensitive to corruption in the data and the model assumptions from which the data has been taken.

The origin of our inverse problem is as follows. For a number of important geophysical investigations from solid earth geophysics to physical oceanography, one needs to know the gravity field of the Earth, or geopotential, with a greater degree of accuracy and resolution than has been achieved to date.[3] The technique of Satellite to Satellite Tracking (SST) can provide measurements of the geopotential at the satellite height which will be described below. This satellite data can provide a global map, at satellite altitude, of the geopotential. With such a map, methods are needed to determine the potential at (or near) the Earth's surface.

One satellite mission under consideration is for two satellites in circular polar orbits, in the same plane, at the same altitude of 160 km, separated by hundreds of kilometers, tracking each other with an accuracy of 10^{-6} m/sec. To be workable it is assumed that both satellites must be equipped with surface force compensation (so-called drag free) devices. An alternative approach also under consideration would be the use of a gravity gradiometer in a similar orbit. In either case, the gravity field at the Earth's surface is ultimately needed, and the inverse methods developed here would be applicable.

This report will discuss the application of geophysical inverse theory to computing the geopotential of points above the Earth with respect to mass points located on the Earth's surface. The observed data in this context will be actual geopotentials of points located at a greater distance from the Earth than the points at which the geopotentials are to be estimated. This is known as the "downward continuation problem." We begin by describing the Earth's potential (geopotential) at any point (r,ϕ,λ) exterior to any mass as

$$V(r,\phi,\lambda) = GM/r + T(r,\phi,\lambda) \quad . \tag{2}$$

Here $0 \leqslant \phi \leqslant \pi$ is the spherical angle of latitude (assuming $\phi = \pi/2$ is the equator), $0 \leqslant \lambda \leqslant 2\pi$ is the angle of longitude, G is Newton's gravitational constant, and M is the mass of the Earth. The central force term, GM/r, is chosen so that the average of $T(r,\phi,\lambda)$, the anomalous potential, over any external sphere is zero. Now, as general practice in physical geodesy, we concern ourselves with T.

From potential theory,[4] if one knows the potential everywhere on a sphere, then the potential at any point outside that sphere can be obtained from Poisson's Integral Formula as

$$T(r,\phi,\lambda) = \frac{R(r^2 - R^2)}{4\pi} \int_0^{2\pi} \int_0^{\pi} \frac{T(R,\phi',\lambda')}{\rho^3} \sin\phi' \, d\phi' d\lambda' \tag{3}$$

where

$$\rho^2 = r^2 + R^2 - 2Rr\cos(\psi)$$

with

$$\cos\psi = \cos\phi\cos\phi' + \sin\phi\sin\phi'\cos(\lambda - \lambda') \quad .$$

This is our forward problem.

From celestial mechanics, one can compute the perturbation in velocity along the direction of motion (v) due to the anomalous potential (T) as

$$v = \frac{T}{na} - 2n\delta r$$

where n is the satellite mean motion, a is the satellite semi-major axis, and δr is a complicated integral which depends on T among other things. It is known that $T \; na > 2n\delta r$. Therefore, we begin with

$$T = na(v + 2n\delta r_o) \quad , \tag{4}$$

where δr_o is an approximation of δr based on partial knowledge of T. In any event, continuous observation of T can provide a map of T, and associated variances. We now wish to use $T(r,\phi,\lambda)$ to estimate $T(R,\delta,\lambda)$ on (or near) the Earth's surface.

We expect that the density of data and horizontal resolution desired preclude inverting the whole problem in one step. For example, for one degree square resolution, more than 42,000

parameters would be necessary. If orthogonal functions, such as spherical harmonics, were used, more than 64,000 coefficients would have to be determined. One motivation for using inverse theory is to treat the inverse problem locally. That is, to estimate the geopotential at (or near) the Earth's surface, from nearby points on an exterior sphere.

It is clear that our inverse problem of determining $T_R(y) = T(R,\phi,\lambda)$ from observed data $T_r(y) = T(r,\phi,\lambda)$ is linear and can be thus attacked by any number of linear inverse methods. Two methods in particular which have acquired familiarity are the Backus-Gilbert formulation[5,1] and the spectral expansion method.[6,7,1] The Backus-Gilbert approach requires an approximation of an appropriate delta function. This approach is not so practical in our situation for the construction of a reliable and implementable solution since, for each point $y = (\phi,\lambda)$ at which the geopotential T_R is desired, one must approximate a delta function about y. Their method does provide, however, a means for evaluating the significance of the solution (see Reference 1, pp. 43-44). The spectral expansion method is much more suited to the construction of a solution which can be subsequently evaluated at several points, y, and we will pursue this method in our inverse problem.

Most solutions by inverse methods are not unique, and it is necessary to briefly discuss this problem in our context. The question of uniqueness in our formulation is equivalent to the question about the nature of the "annihilator of the kernel." Precisely, the annihilator, A, is defined by

$$A \triangleq \{b(y) \mid \int_{S_R} g(x,y)\, b(y)\, dy = 0\}$$

where S_R is the sphere of radius R. If A is empty, then the solution $T_R(y)$ is unique. We cannot count on this being the case, however, and in fact, A turns out to be infinite dimensional. We must proceed without necessarily having uniqueness, however, and simply be aware of this problem which could offset the data. One possible consequence of nonuniqueness is that even the sign of the estimated potential may be wrong.

This report contains five sections, including the introduction. In Section II we will outline the spectral expansion method and discuss some philosophies concerning its use. Section III contains information regarding the physical structure of the experiments performed using the spectral expansion technique. Section IV follows with a detailed discussion on the computational aspects of the experiments, and we conclude with Section V, which outlines the numerical results and some conclusions that can be made.

II. THE SPECTRAL EXPANSION METHOD

In this section, we will discuss the spectral expansion method and introduce the tools that will be needed for construction of the solution T_R. We will follow Parker's outline (Reference 1, pp. 46-49). Suppose we have a finite number, N, of observed data, each having the form in (3). Then we can write

$$T_r(x_i) = \int_{S_R} g(x_i,y)\, T_R(y)\, dy \qquad i = 1, \ldots, N \quad ,$$

or

$$T_i = \int_{S_R} g_i(y)\, T_R(y)\, dy \qquad i = 1, \ldots, N \quad . \tag{5}$$

If we need to treat corrupt data, then we can assume a distribution for the error and include the "noisy" data from the beginning. We consider (5) weighted by the inverse of the standard error of each measurement, σ_i:

$$\frac{T_i}{\sigma_i} = \int_{S_R} \frac{g_i(y)}{\sigma_i}\, T_R(y)\, dy \qquad i = 1, \ldots, N \quad ,$$

which we will write as

$$T_i' = \int_{S_R} g_i'(y)\, T_R(y)\, dy \qquad i = 1, \ldots, N \quad . \tag{6}$$

Now T_i' is dimensionless with unit variance.

We proceed by introducing a matrix Γ with elements Γ_{ij} formed by integrating the double kernel

$$\Gamma_{ij} = \int_{S_R} g_i'(y)\, g_j'(y)\, dy \quad . \tag{7}$$

Γ is non-negative definite and symmetric, and thus, it can be diagonalized by an orthogonal matrix 0,

$$0^T \Gamma 0 = \Lambda = \mathrm{diag}(\lambda_1, \ldots, \lambda_N) \tag{8}$$

with $\lambda_1 \geq \lambda_2 \geq \ldots \geq \lambda_N \geq 0$. Zero eigenvalues may occur if some g_i' is a multiple of some g_j' with $i \neq j$, but we will disregard this possibility temporarily. The set of eigenvalues is called the "spectrum" of the problem defined by (6).

Consider the functions

$$\psi_i(y) = \lambda_i^{-1/2} \sum_{j=1}^{N} 0_{ji} g_j'(y) \quad . \tag{9}$$

It is easy to verify that the ψ_i's are orthonormal functions; that is

$$\int_{S_R} \psi_i(y)\, \psi_j(y)\, dy = \delta_{ij} \quad ,$$

where δ_{ij} is the Kronecker delta function. Thus we may expand T_R in terms of these functions

$$T_R(y) = \sum_{i=1}^{N} a_i \psi_i(y) + \psi^*(y) \tag{10}$$

where ψ^* belongs to A, the annihilator of the kernel, and

$$\int_{S_R} \psi^*(y)\, \psi_i(y)\, dy = 0$$

for each i. The coefficients, a_i, of this expansion must be

$$a_i = \int_{S_R} \psi_i(y)\, T_R(y)\, dy = \lambda_i^{-1\,2} \sum_{j=1}^{N} 0_{ij} \int_{S_R} g_j'(y)\, T_R(y)\, dy$$

$$= \lambda_i^{-1\,2} \sum_{j=1}^{N} 0_{ji} T_j' \quad . \tag{11}$$

Parker (Reference 1, p. 47) notes that the standard error of each coefficient, a_i, is $\lambda_i^{-1\,2}$ and that each a_i is statistically independent. Thus the coefficients of the orthonormal functions ψ_i increase in uncertainty, and the uncertainty for $\psi^*(y)$ is total. If any zero eigenvalues appear, the functions associated with those eigenvalues should be included in the function ψ^* undetermined by the data because those functions have coefficients which are complete in uncertainty. The functions ', also become more oscillatory as i increases, and so the smoothest parts of T_R are most accurately determined because the coefficients of the smoother functions, ψ_i, are more precise. Thus, when many of the eigenvalues are a small fraction of λ_1, then we can assume that we have a numerically (and physically) poorly posed problem, since in this case many of the coefficients a_i exhibit large variances.

It is conceivable to try and provide a smoothed version of the true T_R, and we can do this by filtering out the functions whose coefficients have large uncertainties. Thus, we have a truncated version of (10)

$$\tilde{T}_R(y) = \sum_{i=1}^{L} a_i \psi_i(y) + \psi^*(y) \qquad \text{with } L \leq N \quad . \tag{12}$$

Unfortunately, it is not easy to determine the proper choice of L which maximizes the accuracy, since the truncated sum (12) no longer fits the data exactly. Parker (Reference 1, pp. 48-49) introduces the squared two-norm misfit of the data as a possible tool to study the effects of truncation. Define

$$\chi^2 \triangleq \sum_{i=1}^{N} (\tilde{T}_i' - T_i')^2 \tag{13}$$

where

$$\tilde{T}_i' = \int_{S_R} g_i'(y)\, \tilde{T}_R(y)\, dy \qquad \text{for each } i \quad .$$

Using (7) and (8), we can derive a more practical expression for χ^2. From (13), we have

$$\begin{aligned}
\chi^2 &= \sum_{i=1}^{N} \left(\sum_{j=L+1}^{N} a_j \int_{S_R} g_i(y)\, \psi_j(y)\, dy \right)^2 \\
&= \sum_{i=1}^{N} \left(\sum_{j=L+1}^{N} \sum_{k=1}^{N} a_j \lambda_j^{-1/2} 0_{kj} \int_{S_R} g_i(y)\, g_k(y)\, dy \right)^2 \\
&= \sum_{i=1}^{N} \left(\sum_{j=L+1}^{N} a_j \lambda_j^{-1/2} (0^T \Gamma)_{ji} \right)^2 \\
&= \sum_{i=1}^{N} \left(\sum_{j=L+1}^{N} a_j \lambda_j^{-1/2} \lambda_j 0_{ji}^T \right)^2 \\
&= \sum_{j=L+1}^{N} \sum_{k=L+1}^{N} \sum_{i=1}^{N} a_j a_k \lambda_j^{1/2} \lambda_k^{1/2} 0_{ji}^T 0_{ik} \\
&= \sum_{j=L+1}^{N} \sum_{k=L+1}^{N} a_j a_k \lambda_j^{1/2} \lambda_k^{1/2} (0^T 0)_{jk} \\
&= \sum_{j=L+1}^{N} a_j^2 \lambda_j \quad .
\end{aligned} \tag{14}$$

Parker (Reference 1, p. 49) suggests choosing L s that χ^2 equals its expected value, or so that $P(\chi^2) = 0.5$. Another suggestion is to choose L so that χ^2 is close to the number of independent data. One must proceed with caution, however, since the proper choice of L is intimately related to the model of the underlying system, as the reader will discover in Section V (where we outline the results of our experiments).

III. THE APPLICATION OF THE SPECTRAL EXPANSION METHOD

Two experiments were conducted. For each experiment, a model problem was developed; the first to accommodate a global setting, and the second to accommodate a local setting.

In the first configuration (representing the global setting), twenty mass points were spaced evenly on the Earth's equator. Each point was assigned a unit mass with alternating sign. Thus, the mean mass anomaly is zero. Then, N sample points were chosen randomly at a constant radius above the Earth within a 10% latitude band of the equator ($\phi_x = \pi/2$). The geopotential of each sample point was then computed with respect to the twenty mass points. Thus, the observed data for the i^{th} sample point is

$$T_i = G \sum_{j=1}^{20} \frac{(-i)^j}{R_{ij}} \tag{15}$$

where R_{ij} is the distance between the (i^{th}) sample point and the j^{th} mass point. G is Newton's gravitational constant. One unit of distance was chosen to be the radius of the Earth, and there G = 1.5362E-06 $units^3$ sec^{-2}. A rough sketch of configuration 1 is shown in Figure 1.

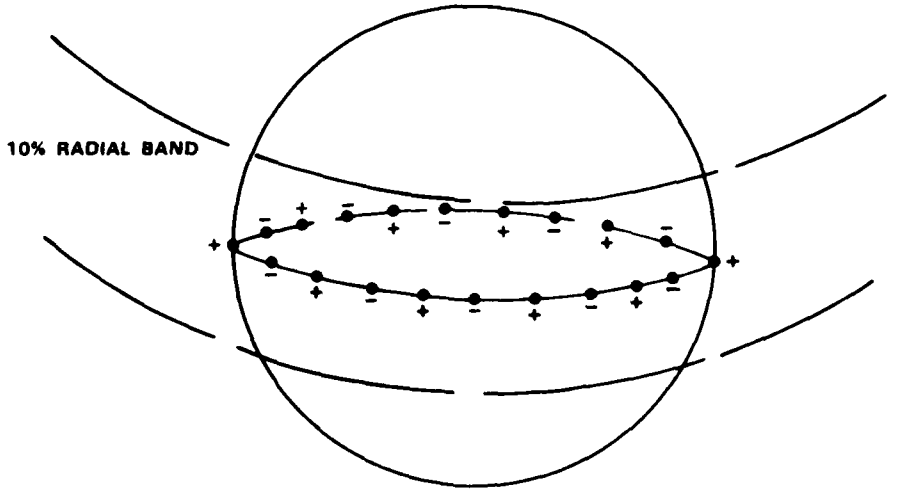

157609-N

Figure 1. Global picture of configuration 1 with mass point structure.

In the second configuration, representing the local setting, we chose a more condensed structure. One mass point was placed at the intersection of the meridian and the equator, and a grid of 24 other mass points was placed around this "origin" with the points spaced at 1° intervals. Each point was assumed to have unit mass with alternating sign as in the first configuration. The structure is shown in Figure 2 with the origin circled.

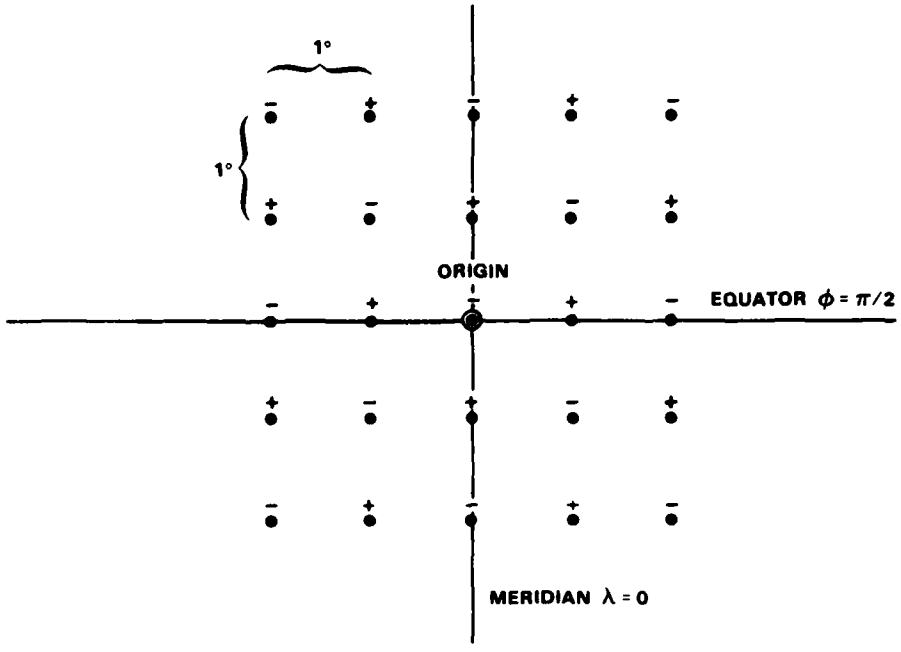

Figure 2. Mass point structure for configuration 2 (regular).

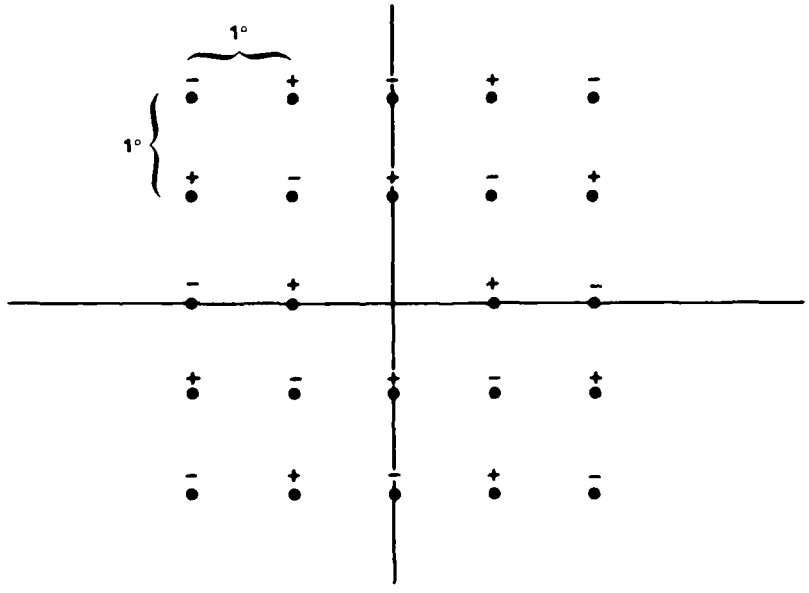

Figure 3. Mass point structure for configuration 2 (alternate).

Now 121 sample points were set up in a similar grid (11 in each row and column) at a constant radius above the Earth directly above the grid of the 25 mass points. Hence the origin of the sample point grid is also at 0 longitude and $\pi/2$ latitude. The geopotential of each sample point was then computed with respect to the 25 mass points similar to (15).

Since the mean mass anomaly of the second configuration is not zero, we created an alternate configuration. We removed the mass at the origin in the grid of the 25 mass points and performed an alternate experiment. In order for the grid to be "isotropic" (invariant under rotation and orientation), the mass points were all assigned the exact sign as in the configuration using all 25 of the mass points (see Figure 3). Sample points were set up in the same way as before.

With each configuration, at a radius, R, strictly between the Earth's radius and the smallest radius at which a sample point was taken, the spectral expansion method is called to yield the geopotential T_R. We ignored ψ^* in (10) and (12), since it is undetermined by the data.

IV. NOTES ON COMPUTATIONS

Before we analyze the results obtained for the experiments performed, it is necessary to understand exactly how the computations were derived. Indeed, since the computations were complicated and involved large matrices, one may look upon the error in the results with some caution rather than if the computations were straightforward. Once the matrix Γ is found, the spectral expansion method required the computation of eigenvalues, eigenvectors, and several finite sums.

The routine used to compute the eigenvalues and eigenvectors was the well-known QL algorithm, a close relative of the QR algorithm. Here L is tridiagonal, which was converted from the original matrix Γ by Householder's method (see Reference 8). This method was chosen for its speed and economy of use of storage space. In the context of large matrices where all the eigenvalues and eigenvectors are needed, we found this method to be more accurate, much faster, and requiring less storage space than other methods such as bisection or the Jacobi method.

It remains to discuss the computation of Γ, (7), and we will give a detailed account. We write (7) explicitly as

$$\Gamma_{ij} = \int_0^{\pi} = \int_0^{2\pi} g(r_i, \phi_i, \lambda_i, r, \phi, \lambda)\, g(r_j, \phi_j, \lambda_j, r, \phi, \lambda)\, R^2 \sin\phi \, d\lambda d\phi$$

$$= \int_0^{\pi} = \int_0^{2\pi} \left[\frac{r_i^2 - R^2}{4\pi R\rho_i^3}\right]\left[\frac{r_j^2 - R^2}{4\pi R\rho_j^3}\right] R^2 \sin\phi \, d\lambda d\phi \qquad (16)$$

with

$$\rho_i^2 = r_i^2 \sim R^2 - 2r_i R \cos\psi_{iy} \quad \text{and} \quad \rho_j^3 = r_j^2 + R^2 - 2r_j R \cos\psi_{jy}$$

where ψ_{iy} is the spherical angle between (ϕ_i, λ_i) and $y = (\phi, \lambda)$. We may rewrite $\cos\psi_{jy}$ using the following well-known law of spherical trigonometry:

$$\cos\psi_{jy} = \cos\psi_{ij} \cos\psi_{iy} + \sin\psi_{ij} \sin\psi_{iy} \cos\alpha \quad , \qquad (17)$$

where α is the angle between the arcs ψ_{ij} and ψ_{iy} (see Figure 4). Now as ϕ and λ range over the whole sphere, α and ψ_{iy} will also range over the whole sphere with $0 \leq \alpha \leq 2\pi$ and $0 \leq \psi_{iy} \leq \pi$, Hence, integrating the double kernel with respect to α and ψ_{iy} will yield an equivalent integral, and we can thus write (16) as

$$\Gamma_{ij} = \int_0^{\pi} \int_0^{2\pi} \left[\frac{r_i^2 - R^2}{4\pi R\rho_i^3}\right]\left[\frac{r_j^2 - R^2}{4\pi R\rho_j^3}\right] \sin\psi_{iy} \, d\alpha \, d\psi_{iy} \quad . \qquad (18)$$

We will proceed to simplify this expression, but first we rename constants as follows:

$$c_1 = \frac{(r_i^2 - R^2)(r_j^2 - R^2)}{16\pi^2} \quad c_2 = r_i^2 + R^2 \;, \; c_3 = r_j^2 + R^2, \; c_4 = -2r_i R \;,$$

$$c_5 = -2r_j R \;, \; c_6 = \cos\psi_{ij} \quad \text{and} \quad c_7 = \sin\psi_{ij} \quad .$$

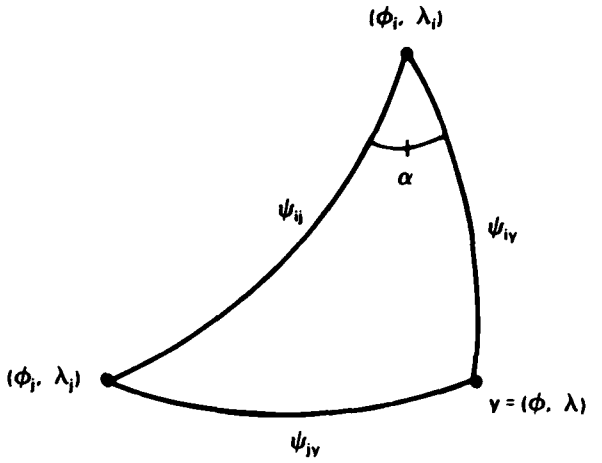

Figure 4. Spherical triangular relationship among points.

We will also write $\psi = \psi_{iy}$. Thus, we write (18) as

$$\Gamma_{ij} = \int_0^{\pi} \int_0^{2\pi} \frac{c_1 \sin\psi \, d\alpha d\psi}{[(c_2 + c_4 \cos\psi)(c_3 + c_5 (c_6 \cos\psi + c_7 \sin\psi \cos\alpha))]^{3/2}} \tag{19}$$

and if we set $a_1(\psi) = c_4 \cos\psi$, $a_2(\psi) = c_3 + c_5 c_6 \cos\psi$, and $a_3(\psi) = c_5 c_7 \sin\psi$, we have

$$\Gamma_{ij} = \int_0^{\pi} \int_0^{2\pi} \frac{c_1 \sin\psi \, d\alpha d\psi}{\left[(c_2 a_2(\psi) + a_1(\psi) a_2(\psi))\left(1 + \frac{a_3(\psi)}{a_2(\psi)} \cos\alpha\right)\right]^{3/2}} . \tag{20}$$

To simplify (17) further, we set $b_1(\psi) = c_1 \sin\psi / [c_2 a_2(\psi) + a_1(\psi) a_2(\psi)]^{3/2}$ and $b_2(\psi) = a_3(\psi)/a_2(\psi)$. Then,

$$\Gamma_{ij} = \int_0^{\pi} b_1(\psi) \int_0^{2\pi} \frac{d\alpha d\psi}{(1 + b_2(\psi) \cos\alpha)^{3/2}} . \tag{21}$$

We leave (21) temporarily and examine the nature of $b_2(\psi)$. Indeed, we will show that $-1 < b_2(\psi) \leq 0$ for all $0 \leq \psi \leq \pi$. Recall

$$b_2(\psi) = \frac{-2r_j R \sin\psi_{ij} \sin\psi}{r_j^2 + R^2 - 2r_j R \cos\psi_{ij} \cos\psi} \tag{22}$$

Since $0 \leq \psi_{ij}, \psi \leq \pi$, the numerator of (22) is always negative (since $r_j, r > 0$). Moreover, $-1 \leq \cos\psi_{ij} \cos\psi \leq 1$ and $r_j > r$ imply that the denominator of (22) is always positive for $0 \leq \psi \leq \pi$ since $r_j^2 + R^2 > 2r_j R$. Thus, $b_2(\psi)$ is always negative for any $0 \leq \psi \leq \pi$. Now, since $-1 \leq \cos(\psi_{ij} - \psi) \leq 1$, it follows that

$$2r_jR\cos(\psi_{ij}-\psi) = 2r_jR[\cos\psi_{ij}\cos\psi + \sin\psi_{ij}\sin\psi] < r_j^2 + R^2 \quad ,$$

which implies that

$$r_j^2 + R^2 - 2r_jR\cos\psi_{ij}\cos\psi > 2r_jR\sin\psi_{ij}\sin\psi \qquad \text{for all } \psi_{ij},\ \psi \quad .$$

Hence $b_2(\psi) > -1$ as claimed.

We ignore ψ for the moment, and we set $a = -b_2(\psi)$ (so that $0 \leqslant a < 1$).

We wish to simplify further:

$$\int_0^{2\pi} \frac{d\alpha}{(1-a\cos\alpha)^{3/2}} = \int_0^{2\pi} \frac{d\alpha}{[1-a(1-2\sin^2\frac{\alpha}{2})]^{3/2}} \tag{23}$$

$$= \int_0^{\pi} \frac{2du}{((1-a)+2a\sin^2 u)^{3/2}} \qquad [\text{where } u = \frac{\alpha}{2}]$$

$$= \frac{4}{(1-a)^{3/2}} \int_0^{\pi/2} \frac{du}{(1+2a\sin^2 u/(1-a))^{3/2}}$$

$$= \frac{4}{(1-a)^{3/2}} \int_0^{\pi/2} \frac{du}{(1+k[1-\cos^2 u])^{3/2}} \qquad [\text{where } k = \frac{2a}{1-a}]$$

$$= \frac{-4}{(1-a)^{3/2}} \int_{\pi/2}^{0} \frac{dy}{((1+k-k\sin^2 y)^{3/2}} \qquad [\text{where } y = \frac{\pi}{2} - u]$$

$$= \frac{4}{(1-a)^{3/2}(1+k)^{3/2}} \int_0^{\pi/2} \frac{dy}{(1-\bar{k}^2\sin^2 y)^{3/2}} \tag{24}$$

$$[\text{where } \bar{k}^2 = \frac{k}{k+1} = \frac{2a}{a+1}].$$

Now (24) is an elliptic integral of the third kind, and if we use formula 17.7.24 in Reference 9, we are able to reduce it to an elliptic integral of the second kind which can be approximated numerically to any degree of accuracy by using well-known techniques. Indeed, (24) can be written as

$$\frac{4}{(1+a)^{3/2}} \sec^2\gamma \int_0^{\pi/2} \sqrt{1-\bar{k}^2\sin^2 y}\, dy \qquad [\text{where } \sin^2\gamma = \bar{k}^2] \tag{25}$$

Since $\sec^2\gamma = (1+a)/(1-a)$, we take as our final form of (23)

$$Y(\psi) = \frac{4}{(1-a)\sqrt{1+a}} \int_0^{\pi/2} \sqrt{1-\frac{2a}{1+a}\sin^2 y}\, dy$$

$$= \frac{4}{(1+b_2(\psi))\sqrt{1-b_2(\psi)}} \int_0^{\pi/2} \sqrt{1+\frac{2b_2(\psi)}{1-b_2(\psi)}\sin^2 y}\, dy \tag{26}$$

where $-1 < 2b_2(\psi)/(1-b_2(\psi)) \leqslant 0$.

There is a vast amount of literature on elliptic integrals, and computation to any degree of accuracy desired is possible by a variety of techniques. We will outline below two methods for computation of $Y(\psi)$, for a given ψ, which are particularly good: a (pseudo)-hypergeometric series expansion and an expansion in terms of theta functions. We will concentrate on the following general form of $Y(\psi)$:

$$E(\bar{k}) = \int_0^{\pi/2} \sqrt{1 - \bar{k}^2 \sin^2 y}\, dy \tag{27}$$

where, in our instance, $\bar{k}^2 = -2b_2(\psi)/(1 - b_2(\psi))$ for a given ψ. Notice that $0 \leq \bar{k}^2 < 1$.

We begin with Grobner and Hofreiter (Reference 10, formula 2b, 2c, p.59)

$$E(\bar{k}) = \sum_{n=0}^{\infty} \binom{1/2}{n} (-\bar{k}^2)\, f_{2n}\left(\frac{\pi}{2}\right) \tag{28}$$

where $f_0(\pi/2) = \pi/2$ and

$$f_{2n}\left(\frac{\pi}{2}\right) = \int_0^{\pi/2} \sin^{2n} y\, dy = \frac{2n-1}{2n} f_{2n-2}\left(\frac{\pi}{2}\right) .$$

Thus,

$$f_{2n}\left(\frac{\pi}{2}\right) = \frac{(1;\ 2;\ n)^n}{2^{n+1}\, n!} \tag{29}$$

where $(1;\ 2;\ n) = 1(1 + 2)(1 + 4)(1 + 6) \ldots (1 + 2(n - 1))$. Now

$$\binom{1/2}{n} (1\ 2)^n = \frac{1}{n!}\left[(1)(-2)(1-4) \ldots (1 - 2(n-1))\right] , \tag{30}$$

and so if we substitute (29) and (30) into (28), we have

$$E(\bar{k}) = \pi \sum_{n=0}^{\infty} (-\bar{k}^2)^n \frac{\left[1(1-2^2)(1-4^2) \ldots (1 - [2(n-1)]^2)\right]}{2^{2n+1}\, (n!)^2} . \tag{31}$$

Equation (31) is the (pseudo)-hypergeometric series representation of (27). The ratio test of (31) yields k^2, and since $0 \leq k^2 < 1$, it does follow that (31) will always converge. If k^2 is quite small, then (31) will be sufficient to give any degree of accuracy desired with only a few terms in the expansion, but as k^2 tends more toward its upper bound, the series (31) converges slower, making it inappropriate for all possible situations. This leads us to a more universal representation of (27): by using theta functions.

We begin by listing the four most common theta functions (Reference 11, p. 464). For z a complex number and $|q| < 1$, define

$$\ell_1(z,q) = 2q^{1/4} \sin z - 2q^{9/4} \sin 3z + 2q^{25/4} \sin 5z \ldots$$

$$= 2 \sum_{n=0}^{\infty} (-1)^n q^{(n+1/2)^2} \sin[(2n+1)z]$$

$$\ell_2(z,q) = 2q^{1/4} \cos z + 2q^{9/4} \cos 3z + 2q^{25/4} \cos 5z \ldots$$

$$= 2 \sum_{n=0}^{\infty} q^{(n+1/2)^2} \cos[(2n+1)z] \quad ,$$

$$\ell_3(z,q) = 1 + 2q \cos 2z + 2q^4 \cos 4z + 2q^9 \cos 6z \ldots$$

$$= 1 + 2 \sum_{n=1}^{\infty} q^{n^2} \cos(2nz) \quad ,$$

and

$$\ell_4(z,q) = 1 - 2q \cos 2z + 2q^4 \cos 4z - 2q^9 \cos 6z + \ldots$$

$$= 1 + 2 \sum_{n=1}^{\infty} (-1)^n q^{n^2} \cos(2nz) \quad .$$

Denote $\ell_2(0,q)$, $\ell_3(0,q)$, and $\ell_4(0,q)$ by ℓ_2, ℓ_3, and ℓ_4, respectively, and write ℓ_1' and ℓ_1''' to denote the first and third derivatives, respectively, of $\ell_1(z,q)$ with respect to z, evaluated at $z = 0$. Whittaker and Watson (Reference 11, p. 467) note

$$\ell_2^4 + \ell_4^4 = \ell_3^4 \quad , \tag{32}$$

and so if we set $\bar{k} = \ell_2^2/\ell_3^2$, then the complement of $\bar{k}$, k ($\bar{k}^2 + k^2 = 1$), satisfies, $\sqrt{k} = \ell_4/\ell_3$. We form $2\epsilon = (1 - \sqrt{k})/(1 + \sqrt{k})$ and note that $0 \leqslant \epsilon < 1/2$ whenever $0 \leqslant \bar{k} < 1$. We follow Reference 11, p. 486 by using ϵ to represent q:

$$q = \epsilon + 2\epsilon^5 + 15\epsilon^9 + 150\epsilon^{13} + 0(\epsilon^{17}) \tag{33}$$

which converges very quickly (usually after only the first three or four terms). Now, if we define $K = 1/2\pi\ell_3^2$, then it can be shown (Reference 11, pp. 499-500), that

$$K = \int_0^{2\pi} \frac{dy}{\sqrt{1 - k^2 \sin^2 y}} \quad , \tag{34}$$

which is an elliptic integral of the first kind. Finally, it can be shown that (27) can be written as

$$E(\bar{k}) = \frac{1}{3} \left\{ 2 - \bar{k}^2 \quad \frac{\ell_1'''}{\ell_3^4 \ell_1'} \right\} K \tag{35}$$

$$= \frac{1}{3} \left\{ 2 - \bar{k}^2 \quad \frac{\ell_1'''}{\ell_2^4 \ell_1'} \right\} \frac{1}{2} \pi \ell_3^2 \, .$$

Now we are given k^2, and so we can use (33) to find an accurate value for q, and then proceed to find ℓ_1''', ℓ_3, and ℓ_1' which can be used to solve for E(k) by using (35). This is the best formulation we have found to yield (27) as accurately as possible given all values of $0 \leqslant \psi \leqslant \pi$.

We continue with our development of computing Γ'_{ij} in its final form:

$$\Gamma'_{ij} = \int_0^{\pi} b_1(\psi)\ Y(\psi)\ d\psi \quad . \tag{36}$$

We evaluated (36) numerically using cautious Romberg extrapolation to find an acceptable estimate of the integral on various subintervals suitably chosen over the given interval $0 \leqslant \psi \leqslant \pi$. We simultaneously solved for $Y(\psi)$ by way of either (31) or (35), depending upon ψ. For both of these integrations we used subroutines developed by the Internationally Mathematical and Statistical Library (IMSL).

Instead of using the Romberg method on the outer integral, we could have used the Gaussian quadrature technique on the interval $[0, \pi]$. This method was tested, and it was found that this technique took much longer than the former method since the integrand is not always well behaved. The Romberg method is often capable of handling jump discontinuities. Whatever method used, one should keep in mind that approximating (36) is more complicated and takes longer as either r_i or r_j approaches R, the radius of the sphere of integration. This may effect the results of the spectral expansion method when sample points are chosen close to the points where T_R is to be estimated.

One final note on computation of the matrix Γ'. If we fix $r_i = r_j = c$, a constant for all i and j, then it is clear that each element Γ'_{ij} will only depend upon the angle between the points $P_i(c, \phi_i, \lambda_i)$ and $P_j(c, \phi_j, \lambda_j)$. There does not seem to be a closed form solution for (36) in this situation, but one method of computing Γ' more rapidly is to calculate Γ'_{ij} for a fraction of the total number of matrix elements, fit a curve through those values corresponding to the angle between P_i and P_j, and interpolate to figure the elements Γ'_{ij} that were not directly computed. We did not do this in our experiments, but this could reduce the computation time considerably if a large number of sample points was involved.

V. NUMERICAL RESULTS

In each experiment, we had the advantage of knowing the true value of the predicted $T_R(y)$ by simply computing the geopotential with respect to the mass points in the same way the observed data were gathered as in (15). This is, of course, not always possible in the situations discussed in the introduction, but the models in our experiments were specifically chosen so that we could test and understand the relevance of inverse theory in the context of computing geopotentials. Hence, we are able to compute a measure of the performance of the inverse theory which is entirely analogous to the Backus-Gilbert method (Reference 1, p. 44). For each test point (R, y_i), after computing the predicted potential $T_R(y_i)$ and the actual potential $T_R(y_i)$, we computed the standard deviation divided by the average value of the actual potentials over the range of sample points:

$$S = \frac{\sum_{i=1}^{N} (\hat{T}_R(y_i) - T_R(y_i))^2}{\sum_{i=1}^{N} T_R^2(y_i)} \tag{37}$$

Considering integral, eigenvalue, and eigenvector approximations, we will be satisfied if our results yield $0 \leqslant S \leqslant 0.2$, and we can conclude that not enough information is contained in the data if $S > 0.2$.

It should be made clear that the inverse routine is computationally expensive, and so before we analyze the results from the experiments, we will briefly discuss the routines and the time involved in executing the routines. The word size of the program with $N = 500$ is close to four million, and so the physical limitations of the computer limit the amount of sample points one can choose. Perhaps a computer that allows more storage space and is faster could make this routine more viable.

Our routine was run on the Harris H800, and Table I lists the time involved for the execution of various aspects of the routine for configuration I with different values of N, the number of sample points, and with the outer sphere containing the sample points as 1.1 and the sphere of

TABLE I

N	CPU Time for Γ	CPU Time Involved for Computation of Eigenvalues and Eigenvectors of Γ
20	18.471 sec	0.417 sec
50	1 min 53.708 sec	6.309 sec
100	7 min 29.639 sec	48.136 sec

TABLE II	
N	S
20	1.17
50	0.98
100	0.77
200	0.48
250	0.41
300	0.35
500	0.196

TABLE III			
N	L	S	χ^2
20	2	0.93	151.4
50	12	0.80	232
100	22	0.69	197
200	147	0.477	1.06

TABLE IV		
N	Largest Eigenvalue	Smallest Eigenvalue
20	24.78332	7.156385
50	45.99	3.00429E-02
100	66.99387	2.31888E-02
200	121.4457	9.078775E-03
250	145.5075	9.0663478E-03
300	147.6130	8.2342017E-03
500	226.612	1.2824643E-03

integration as 1.05. From Table I, we can see that the computation of the eigenvalues and eigenvectors is slightly less than an n^3 problem. This is not surprising since the computation of the eigenvalues and eigenvectors in this case is equivalent to the computation of the inverse of Γ. The computation of Γ itself appears to be slightly less than an n^2 problem, but the computation of Γ takes much longer than the computation of the eigenvalues and eigenvectors of Γ. However, the computation time for Γ will change if one changes the sphere of integration and the sphere at which the sample points were taken (which was held constant), or if one changes the configuration of the sample points. For example, the CPU time involved for computing Γ in configuration 2 with 121 sample points with the outer sphere 1.2 and the inner sphere of integration 1.1 was 6 min 13.523 sec, which is less than in configuration 1 with only 100 sample points taken with the outer sphere and inner sphere 1.1 and 1.05, respectively. The computations in the rest of the routine (coefficients, orthonormal functions, and tests) are linear, and so if one needs a satisfactory upper bound for the total CPU time involved in the routine for the first configuration involving similar parameters with N different, then one should use the total CPU time of 8 min 49.41 sec for N = 100, compute n = N/100, and form $1/3[n + n^2 + n^3]$ 529.41 sec.

In the global setting, configuration 1, there is a direct relationship between the number of sample points used and the tendency of S toward zero; however, the convergence is slow. Consider Table II, which lists S corresponding to varying N.

With each of the cases listed in Table II, we used the radius of the outer sphere and the radius of the inner sphere (of integration) as 1.1 (637.8135 km above the Earth) and 1.05 (318.90675 km above the Earth), respectively. This assumes that the radius of the Earth is 1 unit (6378.135 km).

S was satisfactory only when N was 500 (the upper limit of our program size). So we must consider the effects of truncation as outlined in Section II. The advantage of knowing the actual value, T_R, enabled us to study the effects of using the truncated sum T_R in (12) and the relevance of χ^2 (14). We were able to find the actual L which gave the best value for S. Table III shows some values of N together with the corresponding L which yielded the smallest value of S. The same parameters of radii were used as in Table II. It is easy to see from Table III that an elementary way to choose L in all cases is not likely.

Before any conclusions can be drawn from Table III, it may be helpful to consider the spectrum of the eigenvalues for the various values of N. Table IV lists for the situations in Table II the corresponding maximum and minimum eigenvalue. Figures 5 to 8 show the spectra for the situations listed in Table III, where a continuous curve was drawn through the eigenvalues. Notice that not only does the spectrum widen as N increases, but also, as one can see in Figures 5 to 8, that as N increases, the graph of the spectrum resembles more of a scaled $y = 1/x$ curve. This widening of the spectrum indicates that more information is contained in the data. This suggests that, as N increases, the more oscillatory functions in the expansion (10) have a less damaging effect on the estimation of T_R in the global setting.

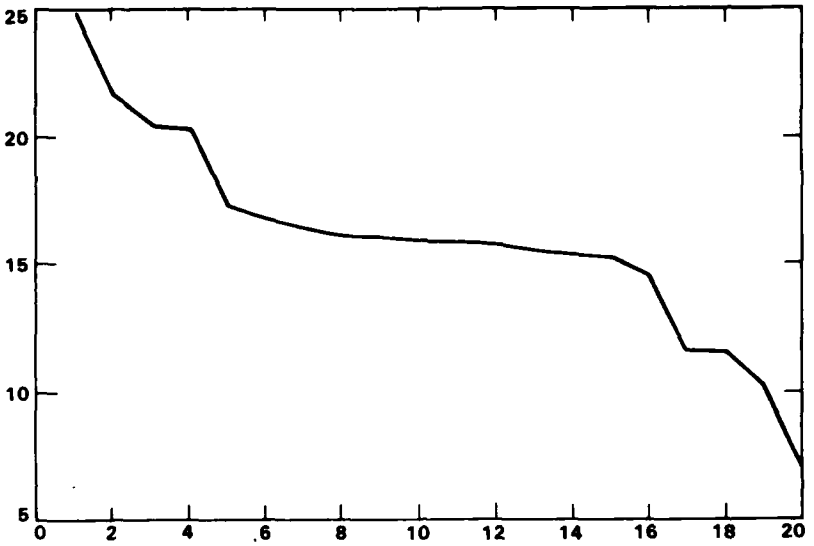

157835-N

Figure 5. Eigenvalue spectrum for configuration 1 with N = 20.

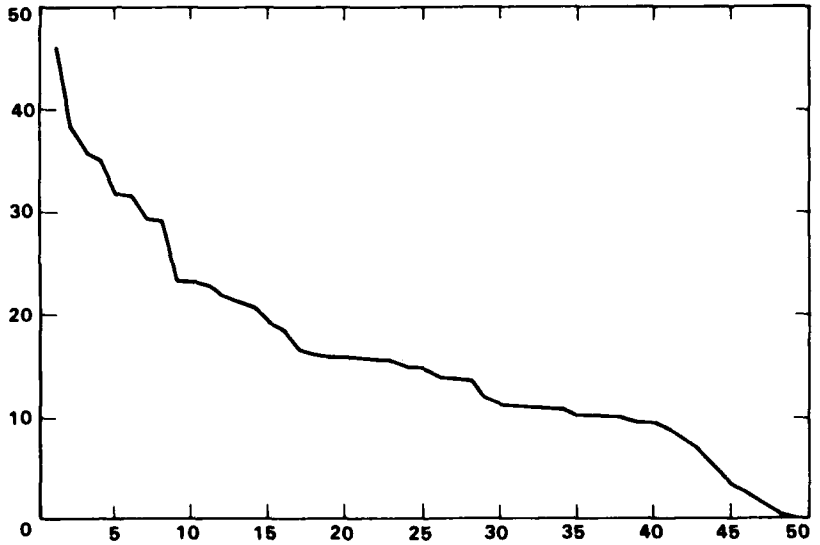

157836-N

Figure 6. Eigenvalue spectrum for configuration 1 with N = 50.

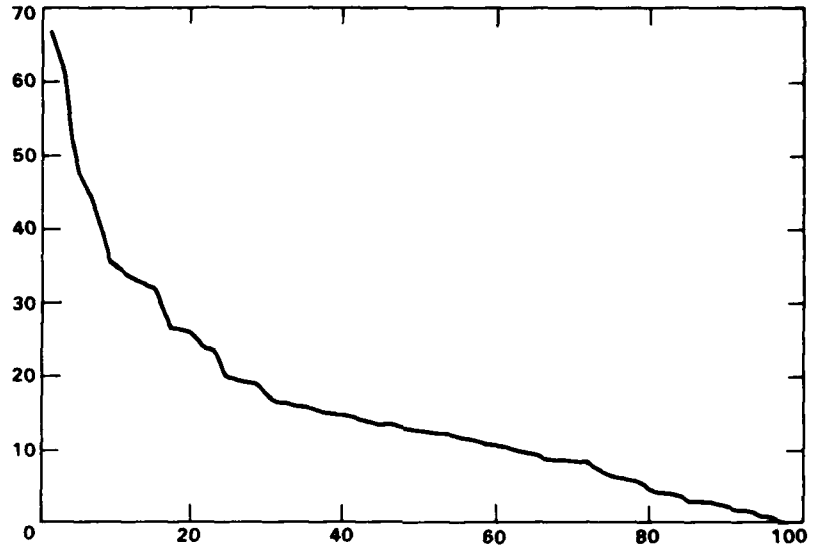

157837-N

Figure 7. Eigenvalue spectrum for configuration 1 with N = 100.

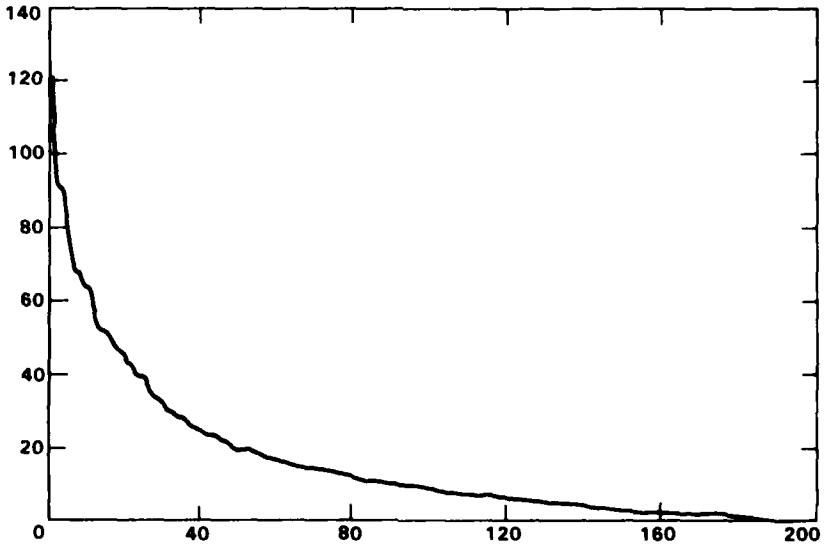

157838-N

Figure 8. Eigenvalue spectrum for configuration 1 with N = 200.

This is supported in Table III. When N is 20, 50, or 100 (where the spectrum is relatively small), L was less than 30% of N and the corresponding values of S were greatly improved. This says that in the global setting when few points are chosen, the oscillatory functions with coefficients exhibiting large uncertainties have a dramatic effect upon the estimation of T_R. When N = 200, L was more than 70% of N and S was only improved by a small amount. Thus, as N increases, our inverse is becoming more stable in the sense that the solution depends continuously (with the two-norm) on the data. Thus the data do not "smooth" T_R as much as N increases, indicating a closer fit. This observation is supported in Parker (Reference 1, p. 42).

Finally, we consider the value of χ^2. Parker (Reference 1, p. 49) conjectures that χ^2 should be chosen close to the number of independent data. This was not found to help in our experiments: for N = 20, 50, or 100, χ^2 was much larger than N, but when N = 200, χ^2 dropped to less than 1% of N. More study is necessary before any information from χ^2 can be extracted to help us select the L yielding the best S.

In configuration 2, we held the number of sample points constant at 121 and varied the radii of the sample point sphere and the sphere of integration. The performance of the routine was much better over all than in the global setting. Consider Table V listing two tests of the experiment: the original configuration is compared with the alternate configuration (where the mean mass anomaly was 0).

TABLE V

Radii	km Above Earth	S with 25 Mass Points Used	S with 24 Mass Points Used
(1) r = 1.1 R = 1.05	637.8135 318.90675	0.15	0.019
(2) r = 1.0333 R = 1.01667	212.60429 106.30182	0.197	0.04

Notice the sensitivity of the theory to the model: the performance of the alternate configuration is certainly as accurate as can be expected while, when 25 mass points were used, S approached its upper acceptable limit. The local configuration consistently out performed the global configuration, even when the mean mass anomaly was not zero. We suspect the poor performance of the nonzero mean configuration is related to the question of uniqueness and the annihilator. See the later discussion of the Stokes integral. This makes a strong argument for the local configuration (especially the alternate configuration) as a setting for a solution to the downward continuation problem. Not only are the results extremely satisfactory, but also the size of the required program is much smaller than the size of the program needed for a similar accuracy in the global setting. Furthermore, truncation of the expansion for T_R in the local setting does little to change the value of S.

This can be explained by once again considering the spectrum of the eigenvalues. Because of the condensed structure of the sample points, the spectrum is much wider than in a similar situation in the global setting. For example, when r = 1.1 and R = 1.05, the eigenvalues ranged between 786.6018 and 1.7198E-04, and the spectrum is shown in Figure 9; when r = 1.0333 and R = 1.01667, the eigenvalues ranged betwen 1843.756 and 3.5439, and the spectrum is shown in Figure 10. One can see from Figures 9 and 10 that the curves outlining the spectra resemble more of a scaled y = 1 x curve, even though only 121 sample points were chosen. Thus stability of the local inversion is better than in the global setting with similar parameters. We can conclude that by using all of the eigenvalues in the expansion (10), we will be obtaining a solution close to the best possible solution based on the data.

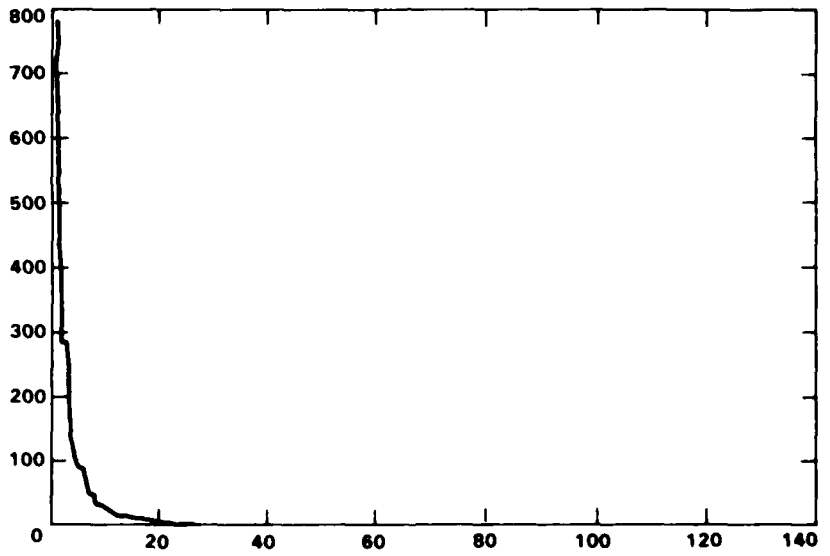

157833-N

Figure 9. Eigenvalue spectrum for configuration 2 (N = 121) with r = 1.1 and R = 1.05.

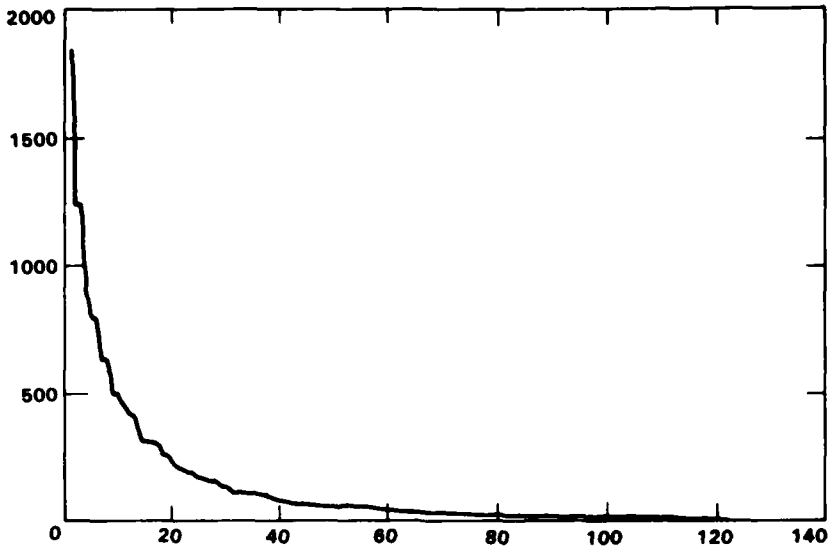

157834-N

Figure 10. Eigenvalue spectrum for configuration 2 (N = 121) with r = 1.0333 and R = 1.01667.

TABLE VI

N	Mean of T_R	Mean of T_R
20	-3.78947E-06	-1.90778E-06
50	1.10474E-06	8.13508E-07
100	1.68239E-06	1.3235E-08
200	9.54483E-08	3.9008E-08

One concern about the results in Table V is that the results tended to consistently get worse as we moved the outer sphere closer to the inner sphere of integration. Our intuition would predict the opposite pattern. The only apparent explanation seems to be that the integral approximations were less accurate as r approached R, and so the results may be misleading.

We conclude this report with a discussion on the relevance of zero means in the functions $\hat{T}_R$ and T_R. Often in physical geodesy, we must consider the consequences of the mean value of the geopotential as it ranges over a (finite) set of data. For example, consider the classical formula of Stokes

$$N = \int S(\psi)\ \Delta g\ d\psi \tag{38}$$

where Δg is the gravitational force field of the Earth, S is the kernel, and N is the integral transformation. Δg has zero mean over the global range, but locally Δg often fails to have zero mean. Furthermore, Δg exhibiting zero mean does not imply that N will also have zero mean. In problems using (38), it is sometimes necessary to consider a global enough setting so that the zero mean is achieved. Our situation seems to behave in a similar fashion. In the local setting, the results strongly showed that the estimate T_R and the actual T_R do not have zero means. In fact, the local structure seems to force a vast majority of the values to be on the same side of zero. However, in the global configuration, we see a tendency more toward zero mean (see Table VI), but more sample points (say 1000 or more) would be needed in order to understand how the means effect the results.

VI. SUMMARY

1. Geophysical Inverse Theory, thus far, seems a viable method to solve the downward continuation problem, and map the geopotential from satellite altitudes to the Earth's surface.

2. The method seems able to recover the geopotential at the Earth's surface with an accuracy of a few percent, with the absence of noise.

3. The inverse problem seems appropriately broken up into local networks, which can be solved separately, leading to significant simplification in computing requirements.

4. Further studies are necessary to fully understand the application of Geophysical Inverse theory to this problem. Among others there are:

   (a) The trade-off of size of the sample point space and the solution space.

   (b) The influence of errors in the sample point space, both position and measurement errors.

   (c) The benefit of sample points at different altitudes, in improving the solution, and eliminating possible nonuniqueness.

   (d) Formal understanding of the annihilator, and possible tests for nonuniqueness.

   (e) Applications of this method to actual data.

REFERENCES

1. R.L. Parker, "Understanding Inverse Theory," Ann. Rev. Earth. Planet. Sci. **5**, 35-64 (1977).

2. P.C. Sabatier, "Comparative Evolution of Inverse Problems," NASA Tech. Memo. X-62 (1971), 150 pp.

3. National Academy of Sciences/National Research Council. Report on a dedicated gravitational satellite mission. Panel on Gravity and Sea Level of the Committee on Geodesy, 1979, 53 pp.

4. W.A. Heiskanen and H. Moritz, *Physical Geodesy* (W.H. Freeman and Co., San Francisco, 1967), 364 pp.

5. L.R. Lines and S. Treitel, "Linear Inverse Theory and Deconvolution," Geophysics **47**, No. 8, 1153-1159 (1982).

6. F. Gilbert, "Ranking and Winnowing Gross Earth Data for Inversion and Resolution," Geophys. J.R. Astron. Soc. **23**, 125-128 (1971).

7. D.D. Jackson, "Interpretation of Inaccurate, Insufficient, and Inconsistent Data," Geophys. J.R. Astron. Soc. **28**, 97-110 (1972).

8. C. Reinsch and J.H. Wilkinson, *Linear Algebra* (Springer-Verlag, Berlin, Heidelberg, and New York, 1971), 439 pp.

9. M. Abramowitz and I. Stegun, *Handbook of Mathematical Functions* (Dover Publications, New York, 1985).

10. W. Grobner and N. Hofreiter, *Integraltafel* (Springer-Verlag, Wien, New York, 1975), 166 pp.

11. E.T. Whittaker and G.N. Watson, *A Course of Modern Analysis* (Cambridge University Press, 1927), 608 pp.

UNCLASSIFIED

SECURITY CLASSIFICATION OF THIS PAGE *(When Data Entered)*

REPORT DOCUMENTATION PAGE		READ INSTRUCTIONS BEFORE COMPLETING FORM
1. REPORT NUMBER ESD-TR-85-279	2. GOVT ACCESSION NO.	3. RECIPIENT'S CATALOG NUMBER
4. TITLE *(and Subtitle)* The Estimation of Geopotentials by Way of Geophysical Inverse Theory		5. TYPE OF REPORT & PERIOD COVERED Technical Report 6. PERFORMING ORG. REPORT NUMBER Technical Report 735
7. AUTHOR(s) Mark T. Lane and Edward M. Gaposchkin		8. CONTRACT OR GRANT NUMBER(s) F19628-85-C-0002
9. PERFORMING ORGANIZATION NAME AND ADDRESS Lincoln Laboratory, M.I.T. P.O. Box 73 Lexington, MA 02173-0073		10. PROGRAM ELEMENT, PROJECT, TASK AREA & WORK UNIT NUMBERS Program Element Nos. 12424F and 63428F Project No. 2129
11. CONTROLLING OFFICE NAME AND ADDRESS Air Force Systems Command, USAF Andrews AFB Washington, DC 20334		12. REPORT DATE 27 January 1986 13. NUMBER OF PAGES 42
14. MONITORING AGENCY NAME & ADDRESS *(if different from Controlling Office)* Electronic Systems Division Hanscom AFB, MA 01731		15. SECURITY CLASS. *(of this Report)* UNCLASSIFIED 15a. DECLASSIFICATION DOWNGRADING SCHEDULE

16. DISTRIBUTION STATEMENT *(of this Report)*

Approved for public release; distribution unlimited.

17. DISTRIBUTION STATEMENT *(of the abstract entered in Block 20, if different from Report)*

18. SUPPLEMENTARY NOTES

None

19. KEY WORDS *(Continue on reverse side if necessary and identify by block number)*

geoid
geopotential
metric data
satellite to satellite tracking
inverse theory
geophysical inverse theory
elliptic integrals
theta functions

20. ABSTRACT *(Continue on reverse side if necessary and identify by block number)*

Satellite to Satellite Tracking data (SST) can be used to measure the geopotential at the satellite altitude. This measurement can be used to estimate the Earth's gravity field at the Earth's surface, the so-called "inverse problem." Geophysical inverse theory is applied to this inverse problem, and numerical methods are developed and tested. Geophysical inverse theory is used to map the geopotential from the satellite altitude to a lower surface. Two configurations are explored and the geopotential in a local network is recovered with less than 4% error.

DD FORM 1 Jan 73 1473 EDITION OF 1 NOV 65 IS OBSOLETE

UNCLASSIFIED

SECURITY CLASSIFICATION OF THIS PAGE *(When Data Entered)*

END

FILMED

4-86

DTIC